

OBSR: Open Benchmark for Spatial Representations

Julia Moska*
 Oleksii Furman*
 Wrocław University of Science and
 Technology
 Department of Artificial Intelligence
 Kraina.AI
 Wrocław, Poland
 julia.moska@pwr.edu.pl

Kacper Kozaczko*
 Szymon Leszkiewicz*
 Jakub Polczyk*
 Kraina.AI
 Wrocław, Poland

Piotr Gramacki
 Piotr Szymański
 piotr.szymanski@pwr.edu.pl
 Wrocław University of Science and
 Technology
 Department of Artificial Intelligence
 Kraina.AI
 Wrocław, Poland

Abstract

GeoAI is evolving rapidly, fueled by diverse geospatial datasets like traffic patterns, environmental data, and crowdsourced Open-StreetMap (OSM) information. While sophisticated AI models are being developed, existing benchmarks are often concentrated on single tasks and restricted to a single modality. As such, progress in GeoAI is limited by the lack of a standardized, multi-task, modality-agnostic benchmark for their systematic evaluation. This paper introduces a novel benchmark designed to assess the performance, accuracy, and efficiency of geospatial embedders. Our benchmark is modality-agnostic and comprises 7 distinct datasets from diverse cities across three continents, ensuring generalizability and mitigating demographic biases. It allows for the evaluation of GeoAI embedders on various phenomena that exhibit underlying geographic processes. Furthermore, we establish a simple and intuitive task-oriented model baselines, providing a crucial reference point for comparing more complex solutions.

CCS Concepts

• Software and its engineering → Software libraries and repositories; • Information systems → Geographic information systems; • Computing methodologies → Machine learning; Learning latent representations; Spatial and physical reasoning; Transfer learning.

Keywords

GeoAI, geospatial, urban, datasets, benchmark, representation learning

ACM Reference Format:

Julia Moska, Oleksii Furman, Kacper Kozaczko, Szymon Leszkiewicz, Jakub Polczyk, Piotr Gramacki, and Piotr Szymański. 2025. OBSR: Open Benchmark for Spatial Representations. In *The 33rd ACM International Conference on Advances in Geographic Information Systems (SIGSPATIAL '25), November 3–6, 2025, Minneapolis, MN, USA*. ACM, New York, NY, USA, 12 pages. <https://doi.org/10.1145/3748636.3762783>

*Equal contribution to the benchmark



This work is licensed under a Creative Commons Attribution 4.0 International License.
 SIGSPATIAL '25, Minneapolis, MN, USA
 © 2025 Copyright held by the owner/author(s).
 ACM ISBN 979-8-4007-2086-4/2025/11
<https://doi.org/10.1145/3748636.3762783>

1 Introduction

The rapid advancements in artificial intelligence (AI) have transformed many industries, thanks in large part to the establishment of robust benchmarking systems that facilitate performance evaluation and comparison. In the realm of geospatial analysis, the emergence of sophisticated AI models has highlighted the critical need for specialized benchmarks tailored to this unique data landscape. This paper introduces a geospatial benchmark designed to assess the performance, accuracy, and efficiency of AI-driven geospatial tools and algorithms. By using standardized metrics and protocols, this benchmark will not only enable objective comparisons among various AI solutions but also encourage innovations that leverage geospatial data.

Geospatial data, essential for these applications, must either represent geometries with coordinates or be geocodable to specific regions or locations. Such data can encompass various forms, including text (e.g., tags, reviews, social media posts, documents), images (e.g., satellite multispectral and hyperspectral imagery, aerial photos, street view images, videos), and numerical values (e.g., weather readings, population statistics, traffic data, point-of-interest ratings). As such most of the existing benchmarks have been limited to a single optimization task ex. location encoding, or modality such ex. satellite imagery. What is however not available is a multi-task benchmark that is agnostic of the modality, featuring an intuitive baseline to compare to - based on basic map-sourced information only.

The contributions of this paper are following:

- (1) review of established open datasets for popular tasks in geospatial research community,
- (2) discussion on what makes a geospatial benchmark work and data processing needed for benchmark creation,
- (3) multi-task, modality agnostic benchmark that allows evaluation of GeoAI models' capability of inference in terms of multiple phenomena that exhibit an underlying geographic process and are well cited in scientific literature,
- (4) natural, simple and intuitive baseline that the authors of large geospatial models can compare to.

We use the SRAI [18] library, which provides a critical resource by focusing on publicly available datasets with clearly defined vector geometries (points, lines, polygons). This focus enhances reproducibility, simplifies usage, and democratizes access to geospatial data, enabling users without extensive GIS expertise to engage with and benefit from geospatial analysis. This library is a natural home for the kind of benchmark we are proposing. Benchmark code is

available in public GitHub repository: <https://github.com/krainai/srai>, where we provide a reproducible experimental code.

2 Related work

In this Section we provide an overview of best practices in benchmarking across different domains and existing geospatial benchmarks. Based on that, we define requirements for a high quality geospatial benchmark and show which gaps we aim to fill with our proposed OCSR benchmark.

2.1 Non-Geospatial Benchmarks

The development of standardized datasets and benchmarks has been fundamental to recent breakthroughs in machine learning and artificial intelligence. Well-established, universally adopted evaluation frameworks have enabled significant progress across domains including Computer Vision and Natural Language Processing. As models demonstrate improved performance on existing datasets, this success drives the creation of more challenging evaluation tasks, creating a virtuous cycle of advancement. With models becoming increasingly capable of handling multiple tasks simultaneously, the focus shifted toward comprehensive multi-task evaluation frameworks. Benchmarks such as GLUE[43] and SuperGLUE[36] established the standard for systematic language model evaluation, an approach subsequently adapted for other languages through initiatives like LEPISZCZE[4] for Polish. Beyond merely aggregating datasets, LEPISZCZE introduced crucial infrastructure improvements including unified access APIs and standardized train/test splits, facilitating reproducible research and rigorous model comparisons. The MTEB[33] and MMTEB[13] benchmarks further demonstrate the potential of comprehensive evaluation frameworks, providing unified interfaces for diverse text embedding tasks while maintaining public leaderboards that enable practitioners to identify optimal models for specific applications.

Computer vision benchmarks illustrate similar design evolution: from ImageNet's[10] emphasis on scale and categorical diversity (14 million images across 20,000 categories) to MS COCO's[28] focus on contextual complexity and task variety (object detection, segmentation, and captioning in natural scenes).

Effective benchmark design principles, demonstrated across NLP and computer vision domains, emphasize domain diversity and real-world contextual complexity that mirrors actual deployment scenarios rather than simplified academic tasks. These design patterns ensure that benchmarks drive meaningful progress by exposing the gap between controlled experimental performance and practical application requirements.

2.2 Geospatial benchmarks

Geospatial community is also developing benchmarks to evaluate models in rapidly developing GeoAI domain, which is starting to develop Geospatial Foundation Models (GeoFM). This leads to new challenges, raised by Mai et al. [30], one of which is the need for a unified set of geospatial tasks to evaluate those GeoFMs on. This need for more geospatial benchmarks was highlighted by the IBM/NASA team that built Prithvi - the first open source GeoFM [21], reiterated by scientists working on Urban Foundation Models (UFM) [55]. Scientists who advocate for coherent experimental

AI research based on scientific principles published a document mentioning the need for new benchmarks recently as well [26].

While reviewing the literature in search of GeoAI benchmarks one can immediately see that existing benchmarks are limited to a single modality and often to a single task or a family of very close tasks.

Computer Vision related geospatial benchmarks are usually dedicated to models that work on remote sensing imagery either satellite-captured or obtained through orthophotography. The authors of TorchGeo[39] noted that many datasets used in geospatial imagery exhibit caveats and errors which require data processing, which was often performed differently by various authors thus reporting results that were non-comparable. As a result, the authors provide a library that, among others, standardizes the dataset preparation and allows comparable benchmarking.

Following the success of ImageNet, the GeoImageNet[27] has been proposed. This dataset focuses on benchmarking the models with respect to their ability to detect various qualities of terrain based on satellite imagery. Another recent satellite imagery benchmark was dedicated to measuring the ability of satellite image segmentation [44].

Earth monitoring benchmarking has been another area of recent advances, which include: Geo-BENCH[23], EarthNets[50], or SustainBench[53]. These benchmarks are in use by most teams that deliver GeoFMs for satellite imagery at global scale.

Shi et al. [38] propose the first benchmark targeted for models that provide inference in terms of estimating various traffic tasks from different scale imagery, including pedestrian detection and vehicle flow counting.

Many problems in GeoAI are related to either textual inference in terms of sequences of spatial data points, or treating spatial sequences as token sequences and applying approaches from Natural Language Processing domain. Several benchmarks have been published in relation to these cases. Xie et al. [47] introduced a benchmark to evaluate a language model's capability to generate a coherent travel itinerary. Aghzal et al. [3] is a benchmark of an LLM's capability to generate sequences of spatial points. Yang et al. [52] proposes a benchmark to evaluate the capability of language models to perform spatial reasoning and comprehension.

Finally, TorchSpatial[46] recently proposed an image-based benchmark for evaluating the efficiency of location embedding.

To summarise, there are already some high-quality benchmarks in the geospatial domain, however there is a crucial gap that needs to be addressed. A vast majority of existing benchmarks focus on remote sensing data and tasks. While they cover some vital applications, their applicability to urban-related tasks is limited. Therefore, there is a need for a benchmark designed with other modalities in mind, such as vector data from OSM.

3 Benchmark

In this Section we describe the OCSR benchmark in detail. We first define a set of criteria that are essential for high quality geospatial benchmark from two perspectives: (i) general benchmark design and (ii) geospatial specific requirements for urban-related applications. We then follow with a detailed description of tasks which we include in our benchmark. Finally, we present which of the highly

esteemed datasets we used to compile our benchmark and how they were processed to create a coherent benchmark.

3.1 What is a good geospatial benchmark?

Based on related works and specific geospatial domain characteristics, we extracted a set of requirements which are crucial for a high-quality benchmark:

- Wide range of datasets covering various tasks in the domain. We achieve this by combining well established datasets and unifying access to them using a single library and data format. We also select different tasks and types of geometries.
- Reproducibility is provided by clearly defined train/test splits. We provide both raw data and predefined splits with preprocessing already applied. This makes it easy to rerun experiments and test new models on the same instances of a given problem.
- Granularity across tasks aims to adapt to different types of spatial dependencies. We achieve this by using different H3¹ resolutions to aggregate data and create instances for datasets in our benchmark.
- Accessibility of data and evaluation code. We host all raw and processed data in publicly available HuggingFace repository and provide an extension to the SRAI library, which handles loading and preprocessing datasets. This integration facilitates seamless use of embedding models implemented within the SRAI framework. To ensure broader accessibility, we also offer straightforward mechanisms for evaluating models independently of the SRAI ecosystem.

3.2 Datasets

To construct a comprehensive and representative benchmark, we curate a collection of 7 geospatial datasets that frequently appear in geospatial AI literature and reflect the diversity of real-world spatial data. These datasets encompass various types of geospatial information, including urban infrastructure, human mobility, housing, and public safety. To enhance generalizability and mitigate demographic biases, the selected datasets cover multiple continents, ensuring geographic and socioeconomic diversity across tasks.

Airbnb : Comprises approximately 3.1 million records from 80 cities worldwide, collected between June 5, 2022, and May 18, 2023. Originating from the Airbnb platform², the dataset includes detailed information about short-term rental listings, including geographic location, property characteristics (e.g., room type, price, availability), host activity, and review metrics. To evaluate spatial modeling in diverse urban contexts, six cities from different countries were selected for inclusion in the benchmark. The dataset was preprocessed to remove incomplete entries and underwent exploratory analysis prior to integration. The dataset is available under the CC BY 4.0 license.

House Sales in King County. [2]: Contains approximately 21,000 residential property sales from King County, Washington, recorded between 2014 and 2015. Designed to support the prediction of 2016

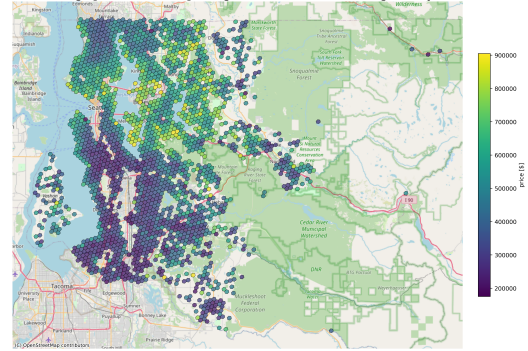


Figure 1: Mean prices per hexagon of houses in King County.

housing prices, the dataset includes geographic coordinates, physical property attributes (e.g., size, number of rooms, condition), and contextual features such as proximity to waterfronts. It enables evaluation of spatial information in price prediction tasks, with clear spatial trends—such as higher prices near the bay—demonstrating the significance of location (Figure 1). The dataset is publicly available under the CC0 license.

Chicago Crime Dataset. [1]: Comprises over 500,000 reported crime incidents (excluding murders) recorded in the City of Chicago between January 2020 and December 2022. The data originates from the Chicago Police Department's CLEAR (Citizen Law Enforcement Analysis and Reporting) system and is publicly available under the CC0 license. Prior to inclusion in the benchmark, records falling outside the city limits were removed as outliers. Each entry includes precise time and location details, supporting fine-grained spatial analysis. Theft is the most frequently reported crime, followed by battery, suggesting patterns linked to tourist activity. Seasonal trends show higher crime rates during summer months, highlighting the importance of spatiotemporal modeling in urban safety analysis. For benchmarking purposes, we used a subset of data originating from the year 2022. Additionally, we provide raw data from multiple years without predefined train-test splits.

Philadelphia Crimes Dataset. ³: Includes approximately 1.5 million recorded crime incidents from the city of Philadelphia. Each entry includes the date, time, and type of crime, enabling spatial and temporal analysis. The dataset serves as a complementary resource to the Chicago Crime Dataset, providing an additional urban context for evaluating geospatial models. It is publicly available under City of Philadelphia License. The benchmark relies on a subset of data originating from crime reports in 2023. Due to licensing restrictions, we provide the train-test splits as lists of IDs.

Police Department Incident Reports Dataset. [11]: Encompasses over 600,000 reported crime incidents submitted by officers or the public through the city's online reporting system. Covering the period from January 2018 to March 2024, it is the most recent dataset among those included in the benchmark. Published under the PDDL license. As with the Chicago and Philadelphia datasets, it provides detailed temporal and categorical information on crimes.

¹<https://www.uber.com/en-PL/blog/h3/>

²<https://insideairbnb.com>

³<https://opendataphilly.org/datasets/crime-incidents/>

Table 1: Summary of datasets included in benchmark. Includes spatio-temporal coverage and number of instances in splits.

	Spatial coverage	Temporal Coverage	res8		res9		res10	
			train	test	train	test	train	test
Airbnb	6 Cities (EU, US, AU)	2022-2023	6648	5535	23148	17105	68166	44397
House sales	King County, US	2014-2015	2098	1368	6323	2770	11280	3305
Chicago crimes	Chicago, US	2022	684	172	3968	992	20200	5051
Philadelphia crimes	Philadelphia, US	2023	425	107	2363	591	11512	2878
Police Dep. Incidents	San Francisco, US	2018-2024	136	35	765	192	3386	847
Porto taxi	Porto, Portugal	2013-2014	-	-	358958	89740	-	-
Geolife	China	2007-2011	-	-	12803	3201	-	-

Porto Taxi. [29]: Captures detailed GPS trajectory data from 442 taxis operating in Porto, Portugal, over a one-year period between July 1, 2013, and June 30, 2014. The dataset is released under CC BY 4.0 license. It was originally collected to support improvements in electronic taxi dispatch systems. Each record corresponds to a completed taxi trip and includes metadata such as trip origin type, taxi and call identifiers, day type, and a GPS trajectory encoded as a sequence of geographic coordinates. The subset used in the benchmark contains nearly 400,000 individual trajectories, providing a rich resource for modeling spatial and temporal mobility patterns in urban environments.

Geolife. [56, 58, 59]: Collected by Microsoft Research Asia from 182 users between 2007 and 2012. It contains over 17,000 trajectories and 25 million GPS points. We filter the data to include only points recorded in Beijing. Each point includes geospatial information, timestamp, and transportation mode (e.g., walking, driving, cycling), enabling multimodal mobility analysis. Due to the dataset’s licensing restrictions, we release train-test splits as lists of trajectory IDs, allowing to match them with the original data.

3.3 Downstream Tasks

Building upon previously defined objectives and an extensive review of the relevant literature, we introduce 5 downstream tasks designed to reflect practical and theoretically meaningful challenges in the field. These tasks fall into two major categories: (1) region-based prediction tasks, where the objective is to estimate values or labels associated with discrete spatial units such as hexagonal grid cells, and (2) trajectory-based tasks, which involve modeling, forecasting, or classifying dynamic movement patterns over space and time. Together, these categories encompass a diverse range of geospatial problems and provide a comprehensive benchmark for evaluating learned spatial representations, while also offering a solid foundation for future extension and methodological development in geospatial machine learning.

3.3.1 Region-based tasks

Short-Term Rental Price Prediction. (STRPP) Short-term rentals have emerged as a significant economic factor in major urban areas in recent years [9, 15, 37, 41]. This growth has spurred research aimed at understanding and potentially leveraging this sector. In particular, predicting rental prices in urban areas has become a critical downstream task in real estate and urban planning research

[20, 25]. To evaluate this task, we propose utilizing data from Airbnb, the widely used short-term rental platform, which offers open access and has been employed in numerous recent studies.

Housing Prices Prediction. (HPP) The prediction of housing prices holds significant societal and economic implications, garnering considerable attention across diverse research disciplines [14, 16]. From a geospatial machine learning perspective, housing prices exhibit strong correlations with a multitude of factors, including location, area, and population demographics, necessitating a comprehensive approach to model individual housing price fluctuations. This complexity has spurred the exploration of advanced machine learning techniques for improved predictive accuracy [32, 42]. We use the House Sales in King County Dataset to facilitate evaluation and comparative analysis in this domain.

Crime Activity Prediction. (CAP) The increasing availability of extensive crime data has spurred scientific interest in the field of crime analysis and prediction, offering potential to aid law enforcement agencies in proactive crime prevention strategies [8]. Real-world crime patterns exhibit strong correlations with temporal, spatial, and demographic factors, introducing complexity into predictive modeling tasks. Machine learning algorithms, capable of incorporating diverse features such as spatial coordinates, time stamps, and population demographics, have shown promise in enhancing predictive accuracy [5, 40, 49]. To support standardized evaluation and benchmarking in this research domain, we adopt three datasets: the Chicago Crime Dataset, the Police Department Incident Reports Dataset and Philadelphia Crimes Dataset. In our formulation, the predictive task is defined as crime intensity estimation. This can be intuitively interpreted as a measure of relative danger or risk level associated with a given geographic region e.g. neighbourhood.

3.3.2 Trajectory-based tasks

Human Mobility Prediction. (HMP) Human mobility prediction, the task of learning and forecasting individuals’ movement trajectories within urban environments, is a fundamental component of numerous location-based services and applications [51]. This field encompasses the characterization of diverse mobility patterns, such as walking, driving, or utilizing public transportation. Understanding these patterns is essential for a wide range of domains, including epidemic control [6, 34], urban planning [48, 54, 57] and traffic forecasting systems [24, 31]. In this study, we address the

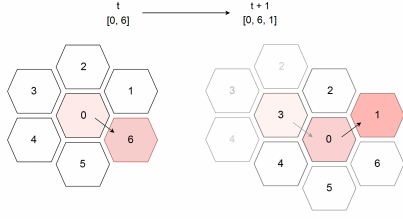


Figure 2: Spatially consistent class-encoding scheme in which each hexagon is encoded relative to its predecessor.

task of human mobility prediction as a autoregressive classification task utilizing widely adopted Geolife and Porto Taxi.

Travel Time Estimation. (TTE) is a critical component of modern transportation systems, increasingly utilized as a fundamental service in navigation and intelligent transportation systems [19, 22]. We propose the utilization of the aforesaid Porto Taxi dataset for time travel estimation analysis as well as Geolife Dataset.

3.4 Data preprocessing

Extensive preprocessing was undertaken to ensure data quality, model robustness, and consistency across tasks. This included the removal of outliers, normalization of numerical variables, and the encoding of categorical attributes to ensure standardized input formats suitable for machine learning models. Preprocessing procedures were further tailored to the nature of the task categories. For region-based tasks such as STRPP, HPP, and CAP, spatial point data were aggregated within predefined hexagonal cells. In STRPP and HPP, average target values (pricing) were computed per cell to form the predictive targets. In the case of CRIME ACTIVITY PREDICTION, the aggregated count of reported crime incidents within each hexagonal cell was interpreted as a measure of crime intensity, serving as a quantitative proxy for the relative safety of a given area. These intensity values were subsequently normalized to a continuous range [0,1] to facilitate comparability and model convergence.

In contrast, for trajectory-based tasks, sequential point data were transformed into paths over a hexagonal spatial grid. While this approach has its advantages and limitations, it allows us to leverage datasets with varying sampling frequencies and temporal resolutions, facilitates spatial aggregation, and improves the comparability of trajectories derived from heterogeneous data sources. Gaps in trajectories—caused by missing or noisy location data—were addressed by estimating intermediate hexagons using shortest-path interpolation and imputing missing feature values based on adjacent valid segments. Furthermore, for HUMAN MOBILITY PREDICTION task (next region classification), we adopt a spatially consistent class-encoding scheme in which each hexagon is encoded relative to its predecessor. Spatial transitions are represented as class labels derived from a fixed directional mapping (Figure 2), ensuring consistency and enabling the model to learn movement dynamics in a localized and coherent frame of reference.

These preprocessing steps established a coherent spatial structure and temporal consistency essential for downstream modeling. To support robust model evaluation, we devised task-specific data

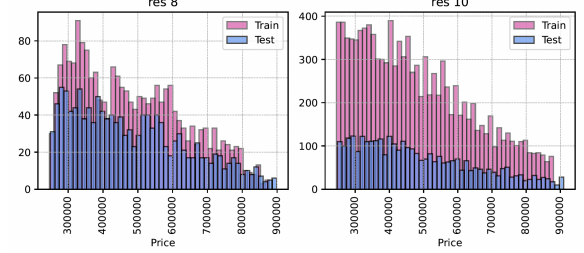


Figure 3: Target feature distribution remains stable for different resolutions in the HPP task.

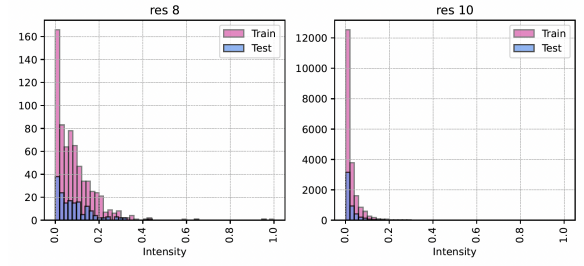


Figure 4: Target feature distribution changes with different resolutions in the CAP task.

partitioning strategies for each category, ensuring reliable and representative training and testing splits. The details of these splitting methodologies are presented in the following section.

3.5 Multi Resolution Configuration

Building on the motivation for granularity adaptation, the benchmark implements a multi-resolution approach using H3 hierarchical hexagonal grid system to create multiple variants of each geospatial task at different spatial scales. This methodology aggregates data using H3 cells of varying resolutions—from coarse-grained large hexagons to fine-grained small ones—enabling comprehensive evaluation of how well models can handle spatial dependencies across different levels of detail. The impact of resolution changes varies significantly depending on the underlying task characteristics and the nature of the target variable. For example, in the HOUSING PRICES PREDICTION and the SHORT-TERM RENTAL PRICE PREDICTION tasks the target feature distribution typically remains stable across resolutions since the underlying spatial patterns are preserved regardless of aggregation scale (see Figure 3). In contrast, for the task of CRIME ACTIVITY PREDICTION, target value systematically decrease as hexagon size decreases, reflecting the mathematical relationship between density measures and the spatial units over which they are calculated (see Figure 4). This multi-resolution framework ensures that geospatial models are evaluated not just on their ability to process spatial data, but on their robustness to the varying scales of spatial aggregation commonly encountered in real-world applications.

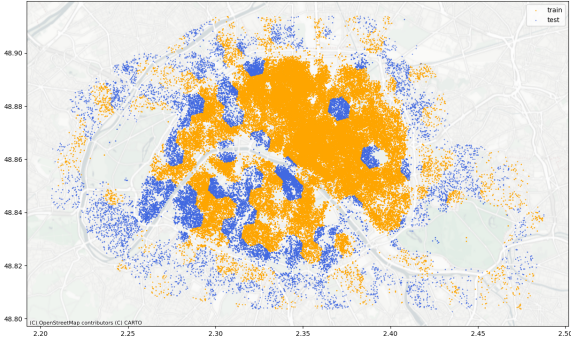


Figure 5: Splitting algorithm ensures no spatial overlap between train and test sets.

3.6 Data Splitting

We support a unified strategy for performing train-test splits in geospatial tasks, where entire hexagonal regions—derived from a predefined spatial resolution—are consistently assigned either to the training or testing set. This ensures that no spatial region appears in both splits, preserving the independence of evaluation. Stratification is applied to maintain balanced distributions of the target variable across the splits. When no explicit target variable is provided (e.g. price), we automatically use the number of points within each hexagonal cell as a proxy, treating it as a measure of local data intensity (e.g. in CAP task). Quantile-based bucketing is then applied to achieve balanced splits while respecting spatial boundaries. This method maintains spatial pattern consistency while enabling better local generalization and is used across all tasks to ensure consistent and reproducible evaluations (see Listing 1 and Figure 5).

For trajectory-based tasks, splitting is performed based on entire sequences to preserve temporal coherence. In the TTE task, trajectories are stratified by their total travel duration to ensure a balanced range of time spans across the training and testing sets. In the HMP task, stratification is based on trajectory length, measured as the number of spatial steps. Each trajectory is subsequently segmented into an input sequence X and a target sequence Y , where Y always corresponds to 15% of the total trajectory length. The train-test split is stratified by trajectory length to ensure a balanced representation of both short and long movement patterns.

To support reproducibility, we provide a collection of precomputed splits at multiple hexagonal resolutions, ready-to-use splitting methods within our library, and access to raw datasets for customized splitting workflows. Detailed statistics of the proposed splits representing the number of regions and trajectories within the train and test splits, are presented in Table 1. The table also summarizes the corresponding spatial and temporal coverage of each split.

4 Evaluation

4.1 Baseline models

To provide reproducible reference points for evaluating spatial representations, we implement a set of simple baseline models. These

models *are not* designed to achieve state-of-the-art performance, but rather to serve as standardized evaluation tools within the benchmark. The primary objective of the provided baselines is to enable the use of *any* available spatial embeddings and to facilitate direct comparisons between them. However, when the focus shifts from benchmarking embeddings to maximizing task-specific performance, these baseline models can be extended or replaced with more sophisticated architectures or end-to-end solutions, and additional metadata from the datasets may be incorporated to improve results.

For price prediction tasks, we employ a feedforward neural network with multiple linear layers and ReLU activations. Conversely, for CAP tasks, sigmoid activation is utilised, with the objective being to attain a range of $[0, 1]$. For sequence-based predictions we employ a recurrent architectures based on LSTM layers, which captures temporal dependencies across variable-length sequences of spatial embeddings. In the case of the TRAVEL TIME ESTIMATION task, the model performs regression based on the entire input sequence. In contrast, for the HUMAN MOBILITY PREDICTION task, the model outputs a class label at each timestep. To enhance sequence modeling in the latter case, we adopt teacher forcing algorithm [17] during training, wherein ground-truth values are used to guide the model's predictions at each step. Additionally, we incorporate a multihead attention layer to effectively capture temporal dependencies and contextual relationships across the entire trajectory. Further details regarding the model architecture and hyperparameters are provided in the appendix A, while the complete implementation is publicly available through the SRAI library.

```
Input: Point dataset G, H3 resolution r, optional target
      y, number of bins n

# 1. Regionalize space into hexagonal cells
Assign each point p in G to an H3 cell h at resolution r

# 2. Define stratification variable
If y is provided:
  Use y values (categorical or numeric) to guide
  stratification
Else:
  Use point counts per H3 cell

# 3. Bucket data for balanced splits
If numeric y or counts:
  Divide values into n quantile-based bins

# 4. Split into train and test sets
Stratify data based on buckets to ensure balanced
  distribution
Assign all points from each H3 cell to the selected split

Return train and test datasets
```

Listing 1: Point-based train-test splitting methods.

4.2 Evaluation methods

To ensure comparable assessment of spatial representations and model performance across the benchmark, we define tailored evaluation strategies for both regression-based and trajectory-based tasks.

For regression tasks, we employ standard error-based evaluation metrics, including the Mean Squared Error (MSE), Root Mean

Table 2: Performance of different embedders on STRPP task on Airbnb dataset at various resolutions. (H2V - Hex2Vec, GV - GeoVex, CE - CountEmbedder, CCE - ContextualCountEmbedder)

Metric	Res 8					Res 9					Res 10		
	H2V	GV	CCE	CE	H2V	GV	CCE	CE	H2V	GV	CCE	CE	
MSE $\times 10^2$	40.10	48.33	40.21	38.30	45.97	50.57	45.65	42.53	59.48	63.80	44.96	66.27	
RMSE	63.33	69.53	63.41	61.89	67.80	71.11	67.50	65.22	77.12	79.87	81.83	81.40	
MAE	43.03	48.58	39.69	39.61	46.97	50.75	42.98	43.21	54.55	56.42	56.96	57.08	
MAPE	51.38	47.47	57.26	58.16	54.17	53.90	60.09	60.90	53.02	51.76	53.53	54.48	
sMAPE	44.49	41.39	48.09	47.88	45.85	44.67	48.67	49.05	46.76	46.76	49.13	49.03	

Table 3: Performance of different embedders on HPP task on House Sales in King County dataset at various resolutions. (H2V - Hex2Vec, GV - GeoVex, CE - CountEmbedder, CCE - ContextualCountEmbedder)

Metric	Res 8					Res 9					Res 10		
	H2V	GV	CCE	CE	H2V	GV	CCE	CE	H2V	GV	CCE	CE	
MSE $\times 10^9$	27.51	26.98	31.69	58.06	23.18	26.82	28.16	26.83	25.28	28.19	22.22	25.22	
RMSE $\times 10^4$	16.577	16.42	17.80	24.09	15.22	16.37	16.77	16.37	15.90	16.78	14.90	15.83	
MAE $\times 10^4$	12.62	13.41	12.95	18.10	11.90	13.38	12.53	12.69	12.56	13.23	11.83	12.62	
MAPE	33.91	30.42	40.26	43.35	33.28	31.64	37.51	33.75	32.22	31.40	34.64	32.68	
sMAPE	33.73	29.23	38.95	46.99	31.67	29.81	36.25	32.22	30.57	30.69	31.81	30.68	

Squared Error (RMSE), and Mean Absolute Error (MAE). In addition, to capture relative predictive performance, we include the Mean Absolute Percentage Error (MAPE), which expresses error as a percentage of the true value. To address the limitations of MAPE in cases where target values approach zero, we also compute the Symmetric Mean Absolute Percentage Error (sMAPE), which symmetrically penalizes over- and under-predictions. These metrics are employed for both the STRPP and HPP tasks, as well as for the TTE task, which—despite being trajectory-based—is also formulated as a regression problem. In the context of the CAP task, where the target variable represents a normalized crime intensity value constrained to the $[0, 1]$ range, percentage-based metrics such as MAPE and sMAPE become unstable and potentially misleading due to their sensitivity to small denominators. Consequently, they are excluded in this particular task and instead the Coefficient of Determination, denoted by R^2 , is incorporated. The R^2 metric is a quantitative measure of the proportion of variance in the dependent variable that is predictable from the independent variables. It offers an interpretable measure of goodness-of-fit for bounded regression tasks.

For HMP task, which require accurate prediction of spatial sequences, we introduce a combination of pointwise and sequence-level metrics:

Average Haversine Distance. : Computes the mean pairwise great-circle distance in meters between corresponding predicted and true H3 cell centroids within each trajectory. This offers a spatially meaningful measure of local deviation in the predicted path.

Dynamic Time Warping (DTW) Distance. : Quantifies the temporal and spatial misalignment between predicted and ground-truth trajectories. Originally developed for time series analysis, DTW [7] allows flexible, non-linear alignment of sequence elements, capturing global shape similarity. In benchmark, we compute the pairwise

distances within DTW using the Haversine formula. It is particularly valuable when evaluating predictions where the same destination is reached via slightly different pacing or intermediate steps, making it a complementary metric to average Haversine distance.

Sequence Accuracy : Measures the proportion of exact element-wise matches between predicted and ground-truth H3 index sequences. This metric provides a straightforward assessment of how often the model predicts the correct location at each step. While intuitive, it is a strict metric—even small spatial or temporal deviations result in lower scores, despite the overall trajectory being reasonably accurate.

As longer sequences naturally increase prediction difficulty, we perform evaluation with these metrics over the first k steps of target trajectory. This approach allows us to granulate task difficulty and better capture model performance at different stages of the prediction horizon.

All of the above, including embedders, task-oriented baseline models and evaluation methods, are fully implemented and readily available as a module in the SRAI library, allowing for consistent, reproducible evaluation across all benchmark tasks. Moreover, they are tightly integrated with the proposed train–test splits for each dataset, enabling researchers to efficiently compute evaluation results of novel geospatial representation learning methods.

4.3 Results

In this Section, we present a comparative evaluation of four geospatial embedding models across multiple spatial analysis tasks, utilizing benchmark datasets of varying resolutions. The reported metrics reflect the average performance across multiple experimental runs to ensure robustness and comparability. In this study, we focus on OSM-based embedders due to the current integration with the SRAI library, which provides native support for these models.

However, the benchmark framework is designed to be fully extensible, allowing the inclusion and comparison of diverse embedders from any modality. The evaluated embedders include:

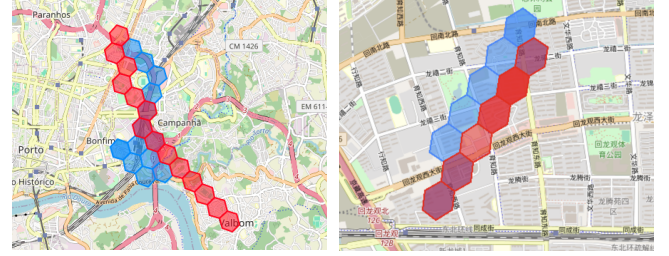
- **Hex2Vec** (H2V) [45], a Skip-gram model with negative sampling, adopted for region embedding pre-training;
- **CountEmbedder** (CE) [35], a frequency-based representation model that encodes OSM features;
- **ContextualCountEmbedder** (CCE) [35], an extension of CountEmbedder that incorporates local spatial context through neighborhood aggregation;
- **GeoVex** (GV) [12], a convolution-based geospatial auto-encoder, which learns region representations from OSM features.

All of the embedding models work on Uber’s H3 cells as regions. Each embedder was applied using consistent preprocessing settings, and with specific parameters that are referenced in Appendix A. Additional dataset features, such as categorical and numerical variables, were deliberately excluded to enable an isolated assessment of geospatial embedding performance, uncontaminated by the influence of other data modalities.

One of the first insights that emerges from the region-based tasks is the critical role of multi-resolution settings. Certain embedders achieve higher accuracy at fine-grained resolutions, yet their performance declines as the spatial units become larger (Table 2, 5), revealing that scalability and spatial sensitivity remain open challenges in geospatial representation learning. This observation underscores the challenges associated with scalability and spatial sensitivity in the context of geospatial learning. As the spatial units increase in size, they have a tendency to aggregate heterogeneous signals. While a proportion of this information may prove useful, a significant amount can become irrelevant or noisy, depending on the nature of the task at hand. In contrast, finer resolutions may necessitate models to capture subtle local variations. Therefore, the ability of an embedder to selectively encode relevant features becomes increasingly important as resolution changes. The current embedding structures and assumptions are sufficiently straightforward in nature to provide a valuable foundation; however, the findings underscore the necessity for more sophisticated, task-specific spatial representation learning methods that can adapt more effectively across diverse scales.

It can be observed that, in the case of the CRIMINAL ACTIVITY PREDICTION task being treated as an intensity prediction within a normalized 0–1 range, the absolute differences between model outputs are naturally constrained, potentially diminishing the significance of performance comparisons. As illustrated in Fig 4, the distribution of target values is skewed, with higher-intensity crime regions being significantly underrepresented in the dataset. The issue becomes more pronounced at coarser spatial resolutions. This imbalance introduces an additional challenge for learning algorithms, which may bias toward predicting low to mid-range intensities to minimize global error (Fig 7, Table 5). Thus, we highlight the importance of using relative improvements and statistical validation to interpret the results meaningfully.

It is also crucial to underline that embedding models evaluated on this benchmark operate with deliberately constrained input



(a) GeoVex, Porto Taxi Dataset (b) Hex2Vec, Geolife Dataset

Figure 6: Human Mobility Prediction task. Predicted sequences in red, gold-answers in blue.

data—utilizing only OSM tag counts from regions, with some models incorporating neighborhood context. While these models lack additional modalities such as satellite imagery or street-view data, they serve as essential baselines for establishing the performance floor that more sophisticated multi-modal approaches should exceed. This baseline approach provides valuable insights into how much performance gain can be attributed specifically to multi-modality versus spatial reasoning capabilities alone. OSM-based feature counts represent a particularly suitable baseline because they offer structured, globally available geospatial information that other modalities typically enhance rather than replace, making performance comparisons meaningful and interpretable. The limitations of these count-based embeddings become most apparent in trajectory-related tasks (see Table 4 and Table 6), where the combination of static regional features with basic sequence models like LSTMs fails to capture the dynamic spatial relationships and movement semantics that define realistic trajectories. This shortcoming is exemplified in Figure 6, where the original trajectory clearly follows established highway infrastructure, but the model’s predictions deviate significantly from road networks, ultimately crossing through forested areas where no viable transportation routes exist.

Table 4: Performance of different embedders on the TTE task for Geolife and Porto Taxi datasets (resolution 9). H2V - Hex2Vec, GV - GeoVex, CE - CountEmbedder, CCE - ContextualCountEmbedder.

Metric	Geolife			
	GV	CCE	CE	
MSE $\times 10^5$	2324.434	2336.848	2336.848	2334.396
RMSE $\times 10^3$	15.246	15.286	15.286	15.278
MAE $\times 10^2$	76.201	76.653	76.653	76.549
MAPE	71.194	69.676	69.676	68.356
Porto Taxi				
MSE $\times 10^5$	1.037	0.954	0.881	0.850
RMSE $\times 10^3$	0.320	0.308	0.296	0.291
MAE $\times 10^2$	1.932	1.911	1.782	1.755
MAPE	37.233	38.863	39.550	40.882

Table 5: Performance of different embedders on CAP task on Chicago Crimes (CC), Philadelphia Crimes (PC) and Police Department Incidents (PDI) datasets at various resolutions. H2V - Hex2Vec, GV - GeoVex, CE - CountEmbedder, CCE - ContextualCountEmbedder

Metric	Res 8				Res 9				Res 10				CC
	H2V	GV	CE	CCE	H2V	GV	CE	CCE	H2V	GV	CE	CCE	
MSE $\times 10^{-3}$	10.093	13.787	7.694	5.840	2.959	4.063	2.475	1.965	1.922	1.984	1.836	1.778	
RMSE $\times 10^{-2}$	10.046	11.741	8.759	7.635	5.440	6.374	4.974	4.431	4.384	4.454	4.285	4.216	
MAE $\times 10^{-3}$	50.685	59.865	44.348	37.100	30.952	36.834	29.442	24.698	20.011	20.629	20.531	19.935	
R2 \uparrow	0.223	-0.060	0.408	0.550	0.339	0.093	0.447	0.561	0.080	0.050	0.121	0.149	
MSE $\times 10^{-3}$	5.458	4.445	3.869	3.422	4.327	4.762	3.528	3.507	2.104	2.162	0.827	0.074	
RMSE $\times 10^{-2}$	7.372	6.675	6.214	5.848	6.578	6.901	5.937	5.922	4.587	4.650	2.876	2.723	
MAE $\times 10^{-3}$	46.967	43.667	39.095	37.989	30.983	34.039	29.811	27.892	18.569	18.888	11.549	11.506	
R2 \uparrow	0.498	0.590	0.644	0.685	0.325	0.257	0.449	0.453	0.075	0.049	0.098	0.191	
MSE $\times 10^{-3}$	20.691	21.111	20.591	19.024	6.544	5.978	4.427	3.543	4.591	4.899	3.420	3.724	
RMSE $\times 10^{-2}$	14.384	14.533	14.348	13.784	8.089	7.733	6.652	5.950	6.775	6.999	5.848	6.102	
MAE $\times 10^{-3}$	70.162	70.633	69.485	64.287	31.947	31.689	28.400	24.798	27.626	27.411	24.297	23.951	
R2 \uparrow	-0.105	-0.128	-0.100	-0.016	0.335	0.393	0.550	0.640	0.204	0.151	0.287	0.354	

Table 6: Performance of different embedders on HMP task for Geolife and Porto Taxi datasets (resolution 9) for different length of sequence k . H2V - Hex2Vec, GV - GeoVex, CE - CountEmbedder, CCE - ContextualCountEmbedder

Metric (avg)	Geolife				Porto Taxi				k
	H2V	GV	CE	CCE	H2V	GV	CE	CCE	
H Dist. [m]	345.44	354.19	309.77	311.67	397.99	439.71	400.35	404.68	
DTW Dist. [m]	345.44	354.19	309.77	311.67	397.99	439.71	400.35	404.68	1
Seq Acc [%] \uparrow	15.203	11.843	8.849	8.383	9.267	13.865	10.507	9.785	
H Dist. (m)	554.02	579.21	449.84	452.79	571.11	644.46	573.23	576.17	
DTW Dist. [m]	1544.26	1614.76	1247.07	1252.05	1530.98	1955.50	1542.14	1550.60	3
Seq Acc [%] \uparrow	7.640	6.637	6.531	5.855	6.584	7.488	7.228	7.111	
H Dist. [m]	705.53	753.66	564.72	565.68	630.75	715.66	633.78	635.68	
DTW Dist. [m]	3049.01	3262.59	2430.33	2422.46	2068.61	2716.54	2084.27	2094.27	5
Seq Acc [%] \uparrow	5.806	5.088	5.562	4.879	6.243	6.949	6.825	6.715	
H Dist. [m]	831.09	898.90	658.36	658.47	654.19	745.39	656.64	658.50	
DTW Dist. [m]	4825.34	5230.19	3807.40	3793.70	2245.80	2958.89	2258.67	2268.14	7
Seq Acc [%] \uparrow	5.070	4.537	5.134	4.477	6.175	6.866	6.746	6.640	
H Dist. [m]	976.77	1063.70	762.80	761.85	665.10	761.06	667.79	669.39	
DTW Dist. [m]	7693.66	8316.19	5970.37	5941.68	2252.10	2967.73	2264.44	2274.48	10
Seq Acc [%] \uparrow	4.545	4.210	4.844	4.243	6.159	6.842	6.722	6.621	

5 Limitations

One key constraint is the limited availability of geospatial embedding models specifically tailored to urban environments and based on rich contextual data such as OpenStreetMap (OSM). Moreover, the few existing models are simplistic in nature, often lacking architectural sophistication or the capacity to capture nuanced urban semantics. As a result, the space of existing approaches available for comparative evaluation is currently narrow, which restricts the diversity of baselines and hinders comprehensive benchmarking.

Furthermore, the proposed trajectory tasks have been evaluated in a single resolution, as this resolution offered an optimal

trade-off between region precision and the necessity of data augmentation (i.e. the augmentation of missing regions). However, given the higher difficulty level exhibited by the trajectory tasks, it is likely that the different resolutions would facilitate a more extensive evaluation context.

It is also important to emphasise that the baseline models incorporated within this benchmark are deliberately elementary and essentially function as reference implementations. While these approaches offer consistency and facilitate comparison, they do not reflect the upper bounds of task performance. More sophisticated modelling strategies may be necessary to capture the full complexity of the benchmark tasks.

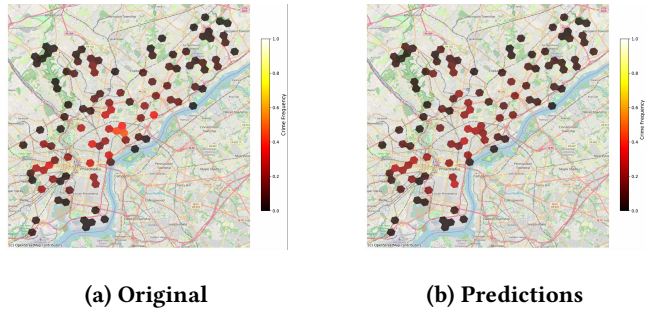


Figure 7: Crime Activity Prediction task on Philadelphia Crimes Dataset using Hex2Vec embeddings.

6 Future works

We aim to expand the benchmark by incorporating additional datasets and introducing new tasks that reflect emerging challenges in geospatial representation learning. The modular design of the accompanying SRAI library allows for seamless integration of such extensions, facilitating community contributions and experimentation. Moreover, we plan to develop a publicly accessible leaderboard that will enable researchers to easily submit and compare results across formulated tasks and datasets. This will foster transparency, reproducibility, and collaborative progress within the geospatial machine learning community. Future work also includes the development of more advanced and task-relevant baseline models to provide stronger reference points and enable more informative evaluation of representation learning methods.

Acknowledgments

Thank you to Kamil Raczycki, Szymon Woźniak and Kacper Leśniara from the Kraina AI team, who supported the technical design of this benchmark. Related Works section was written with the support of deep-research LLM tools. This research was funded in whole or in part by the National Science Centre, Poland grants: Preludium: 2024/53/N/ST6/03296 and Sonata: 2024/55/D/ST6/03082.

References

- [1] 2024. Chicago Crime. <https://www.kaggle.com/datasets/ashkanranjbar/chicago-crime>. Accessed: 2024-05-31.
- [2] 2024. House Sales in King County, USA. <https://www.kaggle.com/datasets/harlfoxem/housesalesprediction/data>. Accessed: 2024-05-31.
- [3] Mohamed Aghzal, Erión Plaku, and Ziyu Yao. 2025. Can Large Language Models be Good Path Finders? A Benchmark and Investigation on Spatial-temporal Reasoning. *arXiv:2310.03249 [cs.CL]* <https://arxiv.org/abs/2310.03249>
- [4] Lukasz Augustyniak, Kamil Tagowski, Albert Sawczyn, Denis Janiak, Roman Bartusiak, Adrian Szymczak, Arkadiusz Janz, Piotr Szymański, Marcin Wątroba, Mikołaj Morzy, Tomasz Kajdanowicz, and Maciej Piasecki. 2022. This is the way: designing and compiling LEPISZCZE, a comprehensive NLP benchmark for Polish. In *Advances in Neural Information Processing Systems*, S. Koyejo, S. Mohamed, A. Agarwal, D. Belgrave, K. Cho, and A. Oh (Eds.), Vol. 35. Curran Associates, Inc., 21805–21818. https://proceedings.neurips.cc/paper_files/paper/2022/file/890b206eb79e550f3988cb8db936f42-Paper-Datasets_and_Benchmarks.pdf
- [5] Fateha Khanam Bappee, Amilcar Soares Júnior, and Stan Matwin. 2018. Predicting crime using spatial features. In *Canadian Conference on Artificial Intelligence*. Springer, 367–373.
- [6] Vitaly Belik, Theo Geisel, and Dirk Brockmann. 2011. Natural human mobility patterns and spatial spread of infectious diseases. *Physical Review X* 1, 1 (2011), 011001.
- [7] Donald J. Berndt and James Clifford. 1994. Using dynamic time warping to find patterns in time series. In *Proceedings of the 3rd International Conference on Knowledge Discovery and Data Mining* (Seattle, WA) (AAAIWS'94). AAAI Press, 359–370.
- [8] Anna L Buczak and Christopher M Gifford. 2010. Fuzzy association rule mining for community crime pattern discovery. In *ACM SIGKDD workshop on intelligence and security informatics*. 1–10.
- [9] Filippo Celata and Antonello Romano. 2022. Overtourism and online short-term rental platforms in Italian cities. In *Platform-Mediated Tourism*. Routledge, 70–89.
- [10] Jia Deng, Wei Dong, Richard Socher, Li-Jia Li, Kai Li, and Li Fei-Fei. 2009. ImageNet: A large-scale hierarchical image database. In *2009 IEEE Conference on Computer Vision and Pattern Recognition*. 248–255. doi:10.1109/CVPR.2009.5206848
- [11] San Francisco Police Department. 2024. Police Department Incident Reports: 2018 to Present. DataSF, City and County of San Francisco. <https://data.sfgov.org/Public-Safety/Police-Department-Incident-Reports-2018-to-Present/wg3w-h783>
- [12] Daniele Donghi and Anna Morvan. 2023. GeoVeX: Geospatial Vectors with Hexagonal Convolutional Autoencoders. In *Proceedings of the 6th ACM SIGSPATIAL International Workshop on AI for Geographic Knowledge Discovery* (Hamburg, Germany) (GeoAI '23). Association for Computing Machinery, New York, NY, USA, 3–13. doi:10.1145/3615886.3627750
- [13] Kenneth Enevoldsen, Isaac Chung, Imene Kerboua, Márton Kardos, Ashwin Mathur, David Stap, Jay Gala, Wissam Siblini, Dominik Krzemieński, Genta Indra Winata, Saba Sturua, Saiteja Utpala, Mathieu Ciancone, Marion Schaeffer, Diganta Misra, Shreyya Dhakal, Jonathan Rystrøm, Roman Solomatin, Ömer Veyse Çağatay, Akash Kundu, Martin Bernstorff, Shitao Xiao, Akshita Sukhlecha, Bhavish Pahwa, Rafał Poświatka, Kranti Kiran GV, Shawon Ashraf, Daniel Auras, Björn Plüster, Jan Philipp Harries, Loïc Magne, Isabelle Mohr, Dawei Zhu, Hippolyte Gisserot-Boukhle, Tom Aarsen, Jan Kostkan, Konrad Wojtasik, Taemin Lee, Marek Suppa, Cristina Zhang, Roberta Rocca, Mohammed Hamdy, Andrianos Michail, John Yang, Manuel Faysse, Aleksei Vatolin, Nandan Thakur, Manan Dey, Dipam Vasani, Pranjal A Chitale, Simone Tedeschi, Nguyen Tai, Artem Sniegirev, Mariya Hendriksen, Michael Günther, Mengzhou Xia, Weijia Shi, Xing Han Lu, Jordan Clive, Gayatri K, Maksimova Anna, Silvan Wehrli, Maria Tikhonova, Henil Shalin Panchal, Aleksandr Abramov, Malte Ostendorff, Zheng Liu, Simon Clematide, Lester James Validad Miranda, Alena Fenogenova, Guangyu Song, Ruqiya Bin Safi, Wen-Ding Li, Alessia Borghini, Federico Cassano, Lasse Hansen, Sara Hooker, Chenghai Xiao, Vaibhav Adlakha, Orion Weller, Siva Reddy, and Niklas Muennighoff. 2025. MMTEB: Massive Multilingual Text Embedding Benchmark. In *The Thirteenth International Conference on Learning Representations*. <https://openreview.net/forum?id=l3pfz4VCV>
- [14] Gregory W Fuller, Alison Johnston, and Aidan Regan. 2020. Housing prices and wealth inequality in Western Europe. *West European Politics* 43, 2 (2020), 297–320.
- [15] Miquel-Ángel García-López, Jordi Jofre-Monseny, Rodrigo Martínez-Mazza, and Mariona Segú. 2020. Do short-term rental platforms affect housing markets? Evidence from Airbnb in Barcelona. *Journal of Urban Economics* 119 (2020), 103278. doi:10.1016/j.jue.2020.103278
- [16] Edward L Glaeser, Joseph Gyourko, and Raven E Saks. 2005. Why have housing prices gone up? *American Economic Review* 95, 2 (2005), 329–333.
- [17] Anirudh Goyal, Alex Lamb, Ying Zhang, Saizheng Zhang, Aaron Courville, and Yoshua Bengio. 2016. Professor forcing: a new algorithm for training recurrent networks. In *Proceedings of the 30th International Conference on Neural Information Processing Systems* (Barcelona, Spain) (NIPS'16). Curran Associates Inc., Red Hook, NY, USA, 4608–4616.
- [18] Piotr Gramacki, Kacper Leśniara, Kamil Raczycki, Szymon Woźniak, Marcin Przymus, and Piotr Szymański. 2023. SRAI: Towards Standardization of Geospatial AI. In *Proceedings of the 6th ACM SIGSPATIAL International Workshop on AI for Geographic Knowledge Discovery*. Association for Computing Machinery. <https://dl.acm.org/doi/10.1145/3615886.3627740>
- [19] YuRui Huang, Jie Zhang, HengDa Bao, Yang Yang, and Jian Yang. 2021. Complementary Fusion of Deep Network and Tree Model for ETA Prediction. In *Proceedings of the 29th International Conference on Advances in Geographic Information Systems*. 638–641.
- [20] Polixeni Iliopoulou, Vassilios Krassanakis, Loukas-Moysis Misthos, and Christina Theodoridi. 2024. A Spatial Regression Model for Predicting Prices of Short-Term Rentals in Athens, Greece. *ISPRS International Journal of Geo-Information* 13, 3 (2024), 63.
- [21] Johannes Jakubik, Sujit Roy, C. E. Phillips, Paolo Fraccaro, Denys Godwin, Bianca Zadrozny, Daniela Szwarcman, Carlos Gomes, Gabby Nyirjesy, Blair Edwards, Daiki Kimura, Naomi Simumba, Linsong Chu, S. Karthik Mulkavilli, Devyani Lambhate, Kamal Das, Ranjini Bangalore, Dario Oliveira, Michal Muszynski, Kumar Ankur, Muthukumaran Ramasubramanian, Iksha Gurung, Sam Khallagh, Hanxi Li, Michael Cecil, Maryam Ahmadi, Fatemeh Kordi, Hamed Aleommamad, Manil Maskey, Raghu Ganti, Kommy Weldenariam, and Rahul Ramachandran. 2023. Foundation Models for Generalist Geospatial Artificial Intelligence. *arXiv:2310.18660 [cs.CV]* <https://arxiv.org/abs/2310.18660>
- [22] Guangyin Jin, Huan Yan, Fuxian Li, Yong Li, and Jincai Huang. 2021. Hierarchical neural architecture search for travel time estimation. In *Proceedings of the 29th International Conference on Advances in Geographic Information Systems*. 91–94.

[23] Alexandre Lacoste, Nils Lehmann, Paul Rodriguez, Evan David Sherwin, Hannah Kerner, Björn Lütjens, Jeremy Irvin, David Dao, Hamed Alemohammad, Alexandre Drouin, Mehmet Gunturkun, Gabriel Huang, David Vazquez, Dava Newman, Yoshua Bengio, Stefano Ermon, and Xiao Xiang Zhu. 2023. GEO-bench: toward foundation models for earth monitoring. In *Proceedings of the 37th International Conference on Neural Information Processing Systems* (New Orleans, LA, USA) (*NIPS* '23). Curran Associates Inc., Red Hook, NY, USA, Article 2223, 14 pages.

[24] Ibai Lana, Javier Del Ser, Manuel Velez, and Eleni I Vlahogianni. 2018. Road traffic forecasting: Recent advances and new challenges. *IEEE Intelligent Transportation Systems Magazine* 10, 2 (2018), 93–109.

[25] JIALIN Li and FILIP Bilecki. 2019. The implementation of big data analysis in regulating online short-term rental business: a case of Airbnb in Beijing. *ISPRS Annals of the Photogrammetry, Remote Sensing and Spatial Information Sciences* 4 (2019), 79–86.

[26] Wenwen Li, Samantha Arundel, Song Gao, Michael Goodchild, Yingjie Hu, Shaowen Wang, and Alexander Zipp. 2024. GeoAI for Science and the Science of GeoAI. *Journal of Spatial Information Science* 29 (2024), 1–17.

[27] Wenwen Li, Sizhe Wang, Samantha T Arundel, and Chia-Yu Hsu. 2023. GeoImageNet: a multi-source natural feature benchmark dataset for GeoAI and supervised machine learning. *GeoInformatica* 27, 3 (2023), 619–640.

[28] Tsung-Yi Lin, Michael Maire, Serge Belongie, James Hays, Pietro Perona, Deva Ramanan, Piotr Dollár, and C. Lawrence Zitnick. 2014. Microsoft COCO: Common Objects in Context. In *Computer Vision – ECCV 2014*, David Fleet, Tomas Pajdla, Bernt Schiele, and Tinne Tuytelaars (Eds.). Springer International Publishing, Cham, 740–755.

[29] Moreira-Matias Luis, Ferreira Michel, Mendes-Moreira Joao, L. L., and J. J. 2015. Taxi Service Trajectory - Prediction Challenge, ECML PKDD 2015. UCI Machine Learning Repository. DOI: <https://doi.org/10.24432/C55W25>.

[30] Gengchen Mai, Yiqun Xie, Xiaowei Jia, Ni Lao, Jinmeng Rao, Qing Zhu, Zeping Liu, Yao-Yi Chiang, and Junfeng Jiao. 2025. Towards the next generation of Geospatial Artificial Intelligence. *International Journal of Applied Earth Observation and Geoinformation* 136 (Feb. 2025), 104368. doi:10.1016/j.jag.2025.104368

[31] Sonu Mathew and Srinivas S Pulugurtha. 2021. Comparative assessment of geospatial and statistical methods to estimate local road annual average daily traffic. *Journal of Transportation Engineering, Part A: Systems* 147, 7 (2021), 04021035.

[32] Thuriaya Mohd, Nur Syafiqah Jamil, Noraini Johari, Lizawati Abdullah, and Suraya Masrom. 2020. An overview of real estate modelling techniques for house price prediction. In *Charting a Sustainable Future of ASEAN in Business and Social Sciences: Proceedings of the 3rd International Conference on the Future of ASEAN (ICoFA) 2019 – Volume 1*. Springer, 321–338.

[33] Niklas Muenninghoff, Nouamane Tazi, Loic Magne, and Nils Reimers. 2023. MTEB: Massive Text Embedding Benchmark. In *Proceedings of the 17th Conference of the European Chapter of the Association for Computational Linguistics*, Andreas Vlachos and Isabelle Augenstein (Eds.). Association for Computational Linguistics, Dubrovnik, Croatia, 2014–2037. doi:10.18653/v1/2023.eacl-main.148

[34] Shunjiang Ni and Wengu Weng. 2009. Impact of travel patterns on epidemic dynamics in heterogeneous spatial metapopulation networks. *Physical review E* 79, 1 (2009), 016111.

[35] Kamil Raczycki and Piotr Szymański. 2021. Transfer learning approach to bicycle-sharing systems' station location planning using OpenStreetMap data. In *Proceedings of the 4th ACM SIGSPATIAL International Workshop on Advances in Resilient and Intelligent Cities* (Beijing, China) (ARIC '21). Association for Computing Machinery, New York, NY, USA, 1–12. doi:10.1145/3486626.3493434

[36] Paul-Edouard Sarlin, Daniel DeTone, Tomasz Malisiewicz, and Andrew Rabivovich. 2020. SuperGlue: Learning Feature Matching With Graph Neural Networks. In *2020 IEEE/CVF Conference on Computer Vision and Pattern Recognition (CVPR)*, 4937–4946. doi:10.1109/CVPR42600.2020.00499

[37] Giovanni Semi and Marta Tonetta. 2021. Marginal hosts: Short-term rental suppliers in Turin, Italy. *Environment and Planning A: Economy and Space* 53, 7 (2021), 1630–1651.

[38] Yifeng Shi, Feng Lv, Xinliang Wang, Chunlong Xia, Shaojie Li, Shujie Yang, Teng Xi, and Gang Zhang. 2023. Open-TransMind: A New Baseline and Benchmark for 1st Foundation Model Challenge of Intelligent Transportation. In *2023 IEEE/CVF Conference on Computer Vision and Pattern Recognition Workshops (CVPRW)*, 6328–6335. doi:10.1109/CVPRW59228.2023.00673

[39] Adam J. Stewart, Caleb Robinson, Isaac A. Corley, Anthony Ortiz, Juan M. Lavista Ferres, and Arindam Banerjee. 2025. TorchGeo: Deep Learning With Geospatial Data. *ACM Trans. Spatial Algorithms Syst.* 11, 4, Article 15 (Aug. 2025), 28 pages. doi:10.1145/3707459

[40] M Raja Suguna, R Beaulah Jeyavathana, and KV Kanimozhi. 2022. Comparative analysis of crime predictions using machine learning algorithms with geospatial features. In *AIP Conference Proceedings*, Vol. 2393. AIP Publishing.

[41] Maxence Valentin. 2021. Regulating short-term rental housing: Evidence from New Orleans. *Real Estate Economics* 49, 1 (2021), 152–186.

[42] Darniton Viana and Luciano Barbosa. 2021. Attention-based spatial interpolation for house price prediction. In *Proceedings of the 29th International Conference on Advances in Geographic Information Systems*. 540–549.

[43] Alex Wang, Amanpreet Singh, Julian Michael, Felix Hill, Omer Levy, and Samuel Bowman. 2018. GLUE: A Multi-Task Benchmark and Analysis Platform for Natural Language Understanding. In *Proceedings of the 2018 EMNLP Workshop BlackboxNLP: Analyzing and Interpreting Neural Networks for NLP*, Tal Linzen, Grzegorz Chrupa, and Afra Alishahi (Eds.). Association for Computational Linguistics, Brussels, Belgium, 353–355. doi:10.18653/v1/W18-5446

[44] Di Wang, Jing Zhang, Bo Du, Minqiang Xu, Lin Liu, Dacheng Tao, and Liangpei Zhang. 2023. Samrs: Scaling-up remote sensing segmentation dataset with segment anything model. *Advances in Neural Information Processing Systems* 36 (2023), 8815–8827.

[45] Szymon Woźniak and Piotr Szymański. 2021. hex2vec: Context-Aware Embedding H3 Hexagons with OpenStreetMap Tags. In *Proceedings of the 4th ACM SIGSPATIAL International Workshop on AI for Geographic Knowledge Discovery (SIGSPATIAL '21)*. ACM, 61–71. doi:10.1145/3486635.3491076

[46] Nemin Wu, Qian Cao, Zhangyu Wang, Zeping Liu, Yanlin Qi, Jielu Zhang, Joshua Ni, X. Angela Yao, Hongxu Ma, Lan Mu, Stefano Ermon, Tanuja Ganu, Akshay Nambi, Ni Lao, and Gengchen Mai. 2024. TorchSpatial: A Location Encoding Framework and Benchmark for Spatial Representation Learning. In *The Thirty-eight Conference on Neural Information Processing Systems Datasets and Benchmarks Track*. <https://openreview.net/forum?id=DERtzUdhkk>

[47] Jian Xie, Kai Zhang, Jiangie Chen, Tinghui Zhu, Renze Lou, Yuandong Tian, Yanghua Xiao, and Yu Su. 2024. TravelPlanner: a benchmark for real-world planning with language agents. In *Proceedings of the 41st International Conference on Machine Learning* (Vienna, Austria) (ICML '24). JMLR.org, Article 2246, 24 pages.

[48] Yanan Xin, Natasa Tagasovska, Fernando Perez-Cruz, and Martin Raubal. 2022. Vision paper: causal inference for interpretable and robust machine learning in mobility analysis. In *Proceedings of the 30th International Conference on Advances in Geographic Information Systems*. 1–4.

[49] Chuanxu Xiong, Ajitesh Srivastava, Rajgopal Kannan, Omkar Damle, Viktor Prasanna, and Errrol Southers. 2019. On predicting crime with heterogeneous spatial patterns: Methods and evaluation. In *Proceedings of the 27th ACM SIGSPATIAL International Conference on Advances in Geographic Information Systems*. 43–51.

[50] Zhitong Xiong, Fahong Zhang, Yi Wang, Yilei Shi, and Xiao Xiang Zhu. 2024. EarthNets: Empowering artificial intelligence for Earth observation. *IEEE Geoscience and Remote Sensing Magazine* (2024), 2–36. doi:10.1109/MGRS.2024.3466998

[51] Hao Xue, Flora Salim, Yongli Ren, and Nuria Oliver. 2021. MobTCast: Leveraging auxiliary trajectory forecasting for human mobility prediction. *Advances in Neural Information Processing Systems* 34 (2021), 30380–30391.

[52] Anran Yang, Cheng Fu, Qingren Jia, Weihua Dong, Mengyu Ma, Hao Chen, Fei Yang, and Hui Wu and. 2025. Evaluating and enhancing spatial cognition abilities of large language models. *International Journal of Geographical Information Science* 0, 0 (2025), 1–36. doi:10.1080/13658816.2025.2490701

[53] Christopher Yeh, Chenlin Meng, Sherrie Wang, Anne Driscoll, Erik Rozi, Patrick Liu, Jihyeon Lee, Marshall Burke, David B. Lobell, and Stefano Ermon. 2021. SustainBench: Benchmarks for Monitoring the Sustainable Development Goals with Machine Learning. In *Thirty-fifth Conference on Neural Information Processing Systems Datasets and Benchmarks Track (Round 2)*. <https://openreview.net/forum?id=5HR3vCylqD>

[54] Jing Yuan, Yu Zheng, and Xing Xie. 2012. Discovering regions of different functions in a city using human mobility and POIs. In *Proceedings of the 18th ACM SIGKDD international conference on Knowledge discovery and data mining*. 186–194.

[55] Weijia Zhang, Jindong Han, Zhao Xu, Hang Ni, Tengfei Lyu, Hao Liu, and Hui Xiong. 2025. Towards Urban General Intelligence: A Review and Outlook of Urban Foundation Models. arXiv:2402.01749 [cs.CY] <https://arxiv.org/abs/2402.01749>

[56] Yu Zheng, Quannan Li, Yukun Chen, Xing Xie, and Wei-Ying Ma. 2008. Understanding mobility based on GPS data. In *Proceedings of the 10th international conference on Ubiquitous computing*. 312–321.

[57] Yu Zheng, Yanchi Liu, Jing Yuan, and Xing Xie. 2011. Urban computing with taxicabs. In *Proceedings of the 13th international conference on Ubiquitous computing*. 89–98.

[58] Yu Zheng, Xing Xie, Wei-Ying Ma, et al. 2010. GeoLife: A collaborative social networking service among user, location and trajectory. *IEEE Data Eng. Bull.* 33, 2 (2010), 32–39.

[59] Yu Zheng, Lizhu Zhang, Xing Xie, and Wei-Ying Ma. 2009. Mining interesting locations and travel sequences from GPS trajectories. In *Proceedings of the 18th international conference on World wide web*. 791–800.

A Architecture & Hyperparameters

All implementations along with exemplary usage notebooks, are publicly available in the SRAI library.

A.1 Embedders

All OSM-based embedders compared in the benchmark use a consistent preprocessing pipeline, including the same OpenStreetMap tag filtering strategy⁴. For both GeoVex and ContextualCountEmbedder, we set the spatial neighborhood size to $k = 2$ to enable aggregation of local features across adjacent H3 cells. The Hex2Vec embedder was configured with encoder layer sizes of [150, 75, 50] for region-based tasks and [150, 75, 25] for trajectory-based tasks, reflecting the different complexity and granularity requirements of the respective inputs.

A.2 STRPP & HPP baseline models

We use a feedforward regression model with hidden layers [50, 100, 50], ReLU activations, and dropout ($p=0.2$) after every second layer. The loss function is Smooth L1 Loss, optimized with Adam ($lr=0.001$). Models were trained for 50 epochs with a batch size of 32.

A.3 CAP baseline model

We utilize the same feedforward architecture as in STRPP and HPP, with hidden layers [50,100,50] and Sigmoid activations. The model

is trained using L1 Loss and optimized with Adam ($lr=0.001$) for 50 epochs with a batch size of 32.

A.4 TTE baseline model

We use a 2-layer LSTM with hidden size 128 and ReLU activation for travel time regression. The input is a sequence of region embeddings, and the model outputs a single scalar as duration. The model is trained with L1 loss and Adam optimizer ($lr=0.001$), batch size 32.

A.5 HMP baseline model

We employed a two-layer LSTM with hidden size 128 followed by multi-head self-attention and a classifier. The model is trained with a hybrid loss: weighted sum of cross-entropy and log-haversine distance (geo loss weight = 0.7). Optimization uses Adam ($lr=0.001$), batch size 32, and 10 epochs. During training, ground truth embeddings are iteratively appended using teacher forcing with embedding lookup. During inference, they are switched to predicted cells.

⁴Following the tag selection procedure from [45], https://github.com/kraina-ai/srai/blob/main/srai/loaders/osm_loaders/filters/hex2vec.py